IRACST – Engineering Science and Technology: An International Journal (ESTIJ), ISSN: 2250-3498, Vol.3, No.1, February 2013

Evaluation of Electromagnetic Fields Exposure During Live Line Working Conditions Inside High Voltage Substations

Samy M. Ghania
Assist. Prof. Elec. Depart., Shoubra faculty of Eng.
Benha University- Cairo, Egypt
Samy_ghania@yahoo.com

Abstract: **The probable risk of electromagnetic fields produced inside high voltage substation is still considered as a competitive topic for utility designers and biomedical field researchers. Hence, the electromagnetic field levels and their induction inside human body should be pre-evaluated as early as the design stage of the substation. This paper deals with the computation of the electromagnetic fields induction in human body inside a typical high voltage 500/220 kV air-insulated substation (AIS). The typical high voltage substation is simulated by developing multi-scripts of m-file Matlab software package to calculate individually both of electric and magnetic fields. Moreover, analytical human body is simulated and allocated within the highly exposure zones of electromagnetic fields. The electromagnetic fields induction inside the human body during live working conditions at different accessible positions is evaluated based on the finite-difference time-domain (FDTD) method for solving Maxwell's equations and the absorbed power density (w/m^2) is calculated using the power density vector (poynting vector).**

Keywords- **High Voltage substations, Electromagnetic fields inductions, Live - line work, FDTD method, Power density vector (poynting vector).**

I- INTRODUCTION

High-voltage power substations are the major part of any utility grid. Power substations with main construction elements (ingoing, bus bars and outgoing lines) are considered effective sources of power frequency (50/60Hz) electromagnetic fields as carrying high voltages and currents [1,2]. Expectedly, power frequency electromagnetic fields produced inside outdoor substations address environmental impact which may cause negative health effects on the workers if there is no attention during the design stage. Some national and international organizations have formulated guidelines establishing the limits for occupational (residential) and general (public) electromagnetic exposure [3-7]. Inside high voltage substations live-line workers are exposed to the electromagnetic fields with considerable strength levels. These electromagnetic fields should be estimated in early stage for safety of workers and the electric current density induced in the worker's body should be evaluated as well [8-10]. Worldwide interest and public concerns of this risk have been tackled for developing advanced numerical algorithms to evaluate electromagnetic fields exposure and induction in different positions for the workers during live maintenance conditions to stand precisely on the exact values for such fields [11, 12]. The worker exposure level and exposure time depend on the different techniques and positions of the workers [13]. Two techniques are used, the first technique is hot-stick working (distance position) in which the worker uses tools mounted on insulating sticks and operates at some safe distance from live elements (3.5m for 500 kV and 2.45 m for 220 kV) [14]. Meanwhile, the second technique is bare-hand working (contact position) in which workers operate in contact directly with the live - line conductors. For the safety purposes the electric and magnetic fields should be estimated in the working zone to ensure compliance with appropriate regulations concerning the occupational exposure to these fields. Workers in bare-hand working operate very close to live conductors and they wear special conductive clothing which protects them against the exposure of the electric field. Unfortunately, this conductive clothing does not protect the live-line worker against the penetration of the magnetic field which consequently induces currents in the worker's body. To avoid adverse health and biological effects in the human organism, the density of this current cannot exceed the exposure limit value of 10 mA/m^2 [6]. The power frequency magnetic field threshold values were established on the basis of the recommendations issued by the International Commission on Non-Ionising Radiation Protection [7] as the magnetic field strength around the live-line worker should not exceed 400 A/m (502.4 μT). This paper presents the electromagnetic fields induction over the worker's body during live working conditions inside high voltage substations. Finite different time domain (FDTD) algorithm is developed to calculate the variation of electric and magnetic field penetrating the worker's vital organs such as brain. Moreover, the induced current density (A/m^2) inside the different parts of the human body is computed as well. The absorbed energy (W/m^2) on the surface area of the different parts of the worker's body is calculated based on the power

density vector (pointing vector). The obtained results are compared with different analytical studies to validate how much of compliance or deviations from international standards.

II- SYSTEM CONFIGURATIONS AND SIMULATION PARAMETERS

A. Substation configurations and worker's positions

The high voltage substation under study is 500/220 kV located in West of Cairo – Egypt territory close to the Alexandria- Cairo desert road. Typically, it consists of four input lines of 500 kV single circuit and 6 output lines of 220 kV double circuits. The higher and lower voltage bus bars are double bus bars horizontal configurations. There are three power transformers each of 500 MVA. The main configurations and the different positions of the workers are simply presented in Figure 1. There are two worker's positions will be considered. The first is at the 1 m above the ground level which presents the position of the workers in the control room during normal operation and (hot-stick position) during live- working conditions. Meanwhile, the second position is at a height of 11 m for 500 kV bus bar and 8.5 m for 220 kV bus bar (bare hand position) during live maintenance conditions.

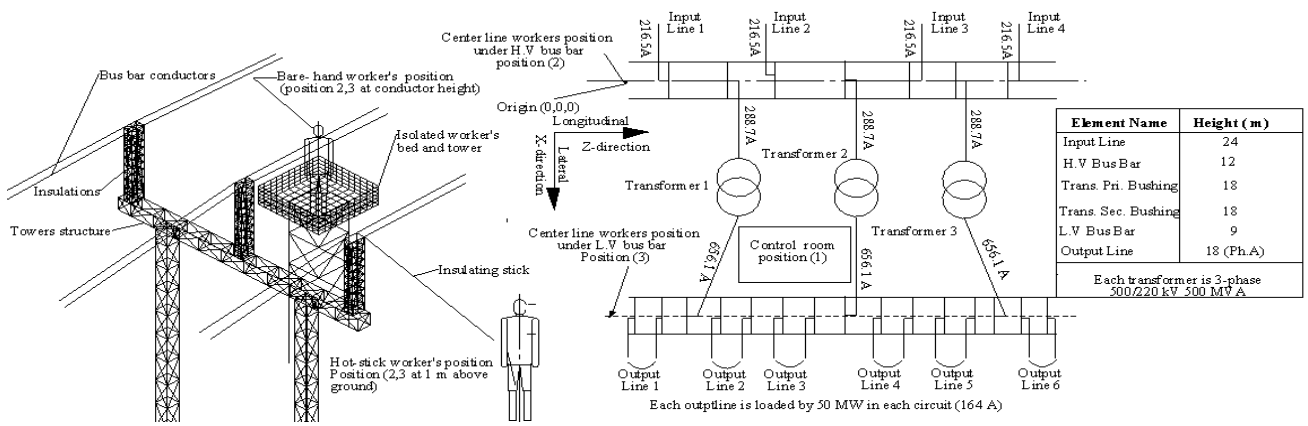

Fig.1: The main parameters of the simulated substation (500/220 kV) and the different positions of the workers during the live-line working conditions

.

B. Electromagnetic fields calculations.

The main power conductors and sub- conductors of the different sections (Input lines - H. V. bus bars – L.V. Bus bars – Output lines) of the substations are simulated with developing many M-Scripts using Matlab software package to calculate individually the emitted magnetic and electric fields. The magnetic field is calculated based on the Biot-Savart law in three dimensions. Figure 2 presents an arbitrary current segment $(\vec{a})$ by which the whole power conductors and sub conductors are divided and connected in series to closely fit the shape of the whole substation in three dimensions. The magnetic field flux density for (n) number of current segments is calculated using Equation 1 [15].

$$\vec{B}(n) = 0.1\vec{I}\left(\frac{\vec{c}\times\vec{a}}{\left|\vec{c}\times\vec{a}\right|^2}\right)\left(\frac{\vec{a}.\vec{c}}{\left|\vec{c}\right|}-\frac{\vec{a}.\vec{b}}{\left|\vec{b}\right|}\right) \quad \mu\text{ Tesla} \qquad (1)$$

For (M) number of conductors and sub conductors the three components and the total magnetic flux density are given as in Equation 2 and 3.

$$\vec{B}_x = \sum_{m=1}^{M}\vec{B}_x(m)$$
$$\vec{B}_y = \sum_{m=1}^{M}\vec{B}_y(m) \qquad \mu\text{ Tesla} \qquad (2)$$
$$\vec{B}_z = \sum_{m=1}^{M}\vec{B}_z(m)$$

$$B_{rms} = \sqrt{B_x^{\,2} + B_y^{\,2} + B_z^{\,2}} \qquad \mu\text{ Tesla} \qquad (3)$$

The electric field intensity is calculated for the main substation power conductors and sub conductors using the charge simulation method (CSM). The developed M-Scripts to simulate the discrete fictitious line charges are used for modeling of the line conductors. These line charges are considered as a proposed solution of Laplace equation which governs the assessment of the electric field [16, 17].

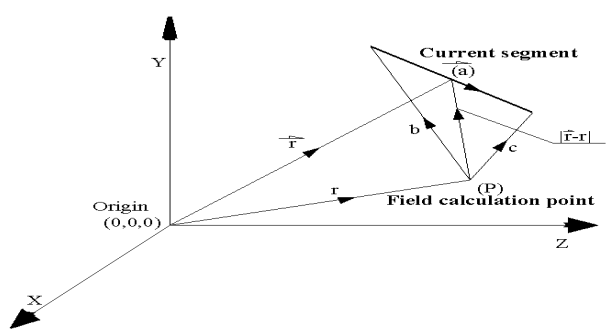

Fig.2: The current segment in free space.

$$[V] = [P]\,[Q] \qquad (4)$$

Figure 3 presents a finite line charge with the check points and some contour points at conductor levels and others at ground level to satisfy the image conditions. The finite line charges are with constant charge densities (Qj) of length (d) between ends at (X1, Y1, Z1) and (X2, Y2, Z2). The potential coefficient (Pij)

at any point Pi (X, Y, Z) due to this charge and its image charge (–Qj) and all other computational equations are given as:

$$\left\{\begin{aligned} P_{ij} &= \frac{1}{4\pi\varepsilon d}\ln\left\{\frac{(L_1+L_2+d)(L_{11}+L_{22}-d)}{(L_1+L_2-d)(L_{11}+L_{22}+d)}\right\} \\ F_x &= \frac{1}{4\pi\varepsilon d}\left\{\left(\frac{X-X_1}{L_1}+\frac{X-X_2}{L_2}\right)\Gamma 1-\left(\frac{X-X_1}{L_{11}}+\frac{X-X_2}{L_{22}}\right)\Gamma 2\right\} \\ F_y &= \frac{1}{4\pi\varepsilon d}\left\{\left(\frac{Y-Y_1}{L_1}+\frac{Y-Y_2}{L_2}\right)\Gamma 1-\left(\frac{Y-Y_1}{L_{11}}+\frac{Y-Y_2}{L_{22}}\right)\Gamma 2\right\} \\ F_z &= \frac{1}{4\pi\varepsilon d}\left\{\left(\frac{Z-Z_1}{L_1}+\frac{Z-Z_2}{L_2}\right)\Gamma 1-\left(\frac{Z+Z_1}{L_{11}}+\frac{Z+Z_2}{L_{22}}\right)\Gamma 2\right\} \end{aligned}\right\} \quad (5)$$

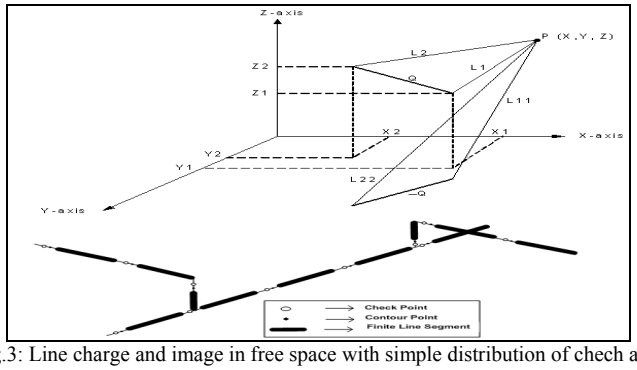

Fig.3: Line charge and image in free space with simple distribution of chech and contour points.

The total electric field intensity (Ei) at any point (Pi) due to a number of individual charges (n) each with charge of (Qj.) is given as:

$$\underline{E}_i = \left[\sum_{j=1}^{n}(F_{ij})_x * Q_j\right]\underline{a}_x + \left[\sum_{j=1}^{n}(F_{ij})_y * Q_j\right]\underline{a}_y + \left[\sum_{j=1}^{n}(F_{ij})_z * Q_j\right]\underline{a}_z \quad (6)$$

Where:

$$\left\{\begin{aligned} &L_1=\sqrt{(X-X_1)^2+(Y-Y_1)^2+(Z-Z_1)^2} && L_2=\sqrt{(X-X_2)^2+(Y-Y_2)^2+(Z-Z_2)^2} \\ &L_{11}=\sqrt{(X-X_1)^2+(Y-Y_1)^2+(Z+Z_1)^2} && L_{22}=\sqrt{(X-X_2)^2+(Y-Y_2)^2+(Z+Z_2)^2} \\ &d=\sqrt{(X_1-X_2)^2+(Y_1-Y_2)^2+(Z_1-Z_2)^2} && \Gamma 1=\frac{1}{(L_1+L_2-d)}-\frac{1}{(L_1+L_2+d)} \\ &\Gamma 2=\frac{1}{(L_{11}+L_{22}-d)}-\frac{1}{(L_{11}+L_{22}+d)} \end{aligned}\right\} \quad (7)$$

c. Worker's body parameters

The worker's body is modeled as a combination of certain elementary geometrical shapes: spheres, cylinders etc. The worker's body main dimensions are given in millimeters [18] and presented as shown in Figure 4. This worker's body model body is allocated at different working positions (hot-stick, bare hand and inside control room). The simulated charges distribution for the human body are simulated as ring charges for the human head, neck, chest and legs while the arms are simulated as finite line charges. The potential is calculated at the location of contour points chosen and consequently the induced electric field components are calculated inside the human body parts.

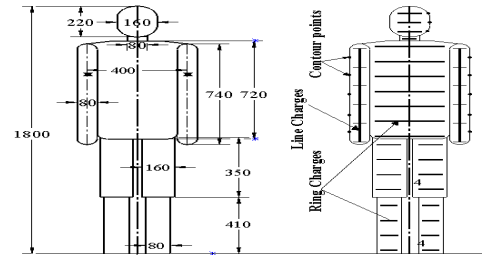

Fig.4: The main dimensions of the worker's body with the types of charges.

D. FDTD basic algorithm's concept

Maxwell's equations for a driving sources and lossy dielectric materials can be presented as in Equation 8. Expanding these two main equations over Yee cell in space with time domain [19-21] yields the main relations of electromagnetic fields in both space and time domain as shown in Figure 5.

$$\left\{\frac{\partial\vec{H}}{\partial t}=-\frac{1}{\mu}\nabla X\vec{E}-\frac{\sigma}{\mu}\vec{H} \quad \text{and} \quad \frac{\partial\vec{E}}{\partial t}+\frac{\sigma}{\varepsilon}\vec{E}=\frac{1}{\varepsilon}\nabla X\vec{H}\right\} \quad (8)$$

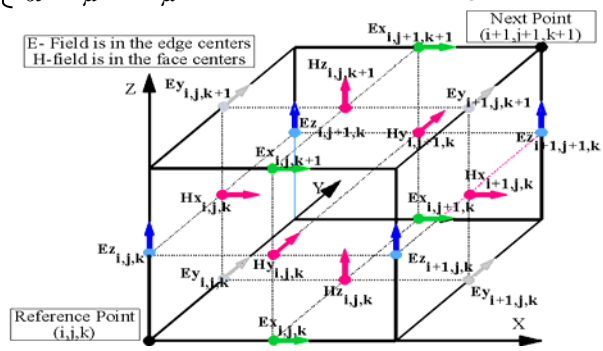

Fig.5: Yee cell presentation for expanding Maxwell's equations at n^{th} node.

Expanding E and H over the Yee cell in space and time domain yields to the following six sub-equations as presented in Equation 9 and Equation10. These six equations present the main standard form to develop FDTD algorithm used to monitor and capture the effects of the distribution of both magnetic and electric field and their duality effects.

$$\left\{\begin{aligned} &\left[\frac{H_y^{(n+1/2)}(i,j,k)-H_y^{(n-1/2)}(i,j,k)}{\Delta x}-\frac{H_x^{(n+1/2)}(i,j,k)-H_x^{(n-1/2)}(i,j,k)}{\Delta y}\right]= \\ &\sigma(i,j,k)\left[\frac{E_z^{(n+1)}(i,j,k)+E_z^{(n)}(i,j,k)}{2}\right]+\varepsilon(i,j,k)\left[\frac{E_z^{(n+1)}(i,j,k)-E_z^{(n)}(i,j,k)}{\Delta t}\right] \\ &\left[\frac{H_z^{(n+1/2)}(i,j,k)-H_z^{(n-1/2)}(i,j,k)}{\Delta y}-\frac{H_y^{(n+1/2)}(i,j,k)-H_y^{(n-1/2)}(i,j,k)}{\Delta z}\right]= \\ &\sigma(i,j,k)\left[\frac{E_x^{(n+1)}(i,j,k)+E_x^{(n)}(i,j,k)}{2}\right]+\varepsilon(i,j,k)\left[\frac{E_x^{(n+1)}(i,j,k)-E_x^{(n)}(i,j,k)}{\Delta t}\right] \\ &\left[\frac{H_x^{(n+1/2)}(i,j,k)-H_x^{(n-1/2)}(i,j,k)}{\Delta z}-\frac{H_z^{(n+1/2)}(i,j,k)-H_z^{(n-1/2)}(i,j,k)}{\Delta x}\right]= \\ &\sigma(i,j,k)\left[\frac{E_y^{(n+1)}(i,j,k)+E_y^{(n)}(i,j,k)}{2}\right]+\varepsilon(i,j,k)\left[\frac{E_y^{(n+1)}(i,j,k)-E_y^{(n)}(i,j,k)}{\Delta t}\right] \end{aligned}\right\} \quad (9)$$

$$\left\{\begin{array}{l}\left[\dfrac{E_z^{(n+1/2)}(i,j,k)-E_z^{(n-1/2)}(i,j,k)}{\Delta y}-\dfrac{E_y^{(n+1/2)}(i,j,k)-E_y^{(n-1/2)}(i,j,k)}{\Delta x}\right]= \\ \sigma(i,j,k)\left[\dfrac{H_x^{(n+1)}(i,j,k)+H_x^{(n)}(i,j,k)}{2}\right]+\mu(i,j,k)\left[\dfrac{H_x^{(n+1)}(i,j,k)-H_x^{(n)}(i,j,k)}{\Delta t}\right] \\ \\ \left[\dfrac{E_x^{(n+1/2)}(i,j,k)-E_x^{(n-1/2)}(i,j,k)}{\Delta z}-\dfrac{E_z^{(n+1/2)}(i,j,k)-E_z^{(n-1/2)}(i,j,k)}{\Delta x}\right]= \\ \sigma(i,j,k)\left[\dfrac{H_y^{(n+1)}(i,j,k)+H_y^{(n)}(i,j,k)}{2}\right]+\mu(i,j,k)\left[\dfrac{H_y^{(n+1)}(i,j,k)-H_y^{(n)}(i,j,k)}{\Delta t}\right] \\ \\ \left[\dfrac{E_y^{(n+1/2)}(i,j,k)-E_y^{(n-1/2)}(i,j,k)}{\Delta x}-\dfrac{E_x^{(n+1/2)}(i,j,k)-E_x^{(n-1/2)}(i,j,k)}{\Delta y}\right]= \\ \sigma(i,j,k)\left[\dfrac{H_z^{(n+1)}(i,j,k)+Hz^{(n)}(i,j,k)}{2}\right]+\mu(i,j,k)\left[\dfrac{H_z^{(n+1)}(i,j,k)-H_z^{(n)}(i,j,k)}{\Delta t}\right]\end{array}\right\} \quad (10)$$

Figure 6 shows the simple presentation of the high-level flow chart of the developed FDTD simulation engine that is typical of the developed FDTD algorithm except for the initialization part. There are many steps in the initialization portion as compared to the basic flow, Furthermore the values are pre-computed and stored in look up tables. Based on the Maxwell's equations extraction the developed algorithm is concerned with calculating the total electric and magnetic field inside the main parts of the worker's body during live working conditions.

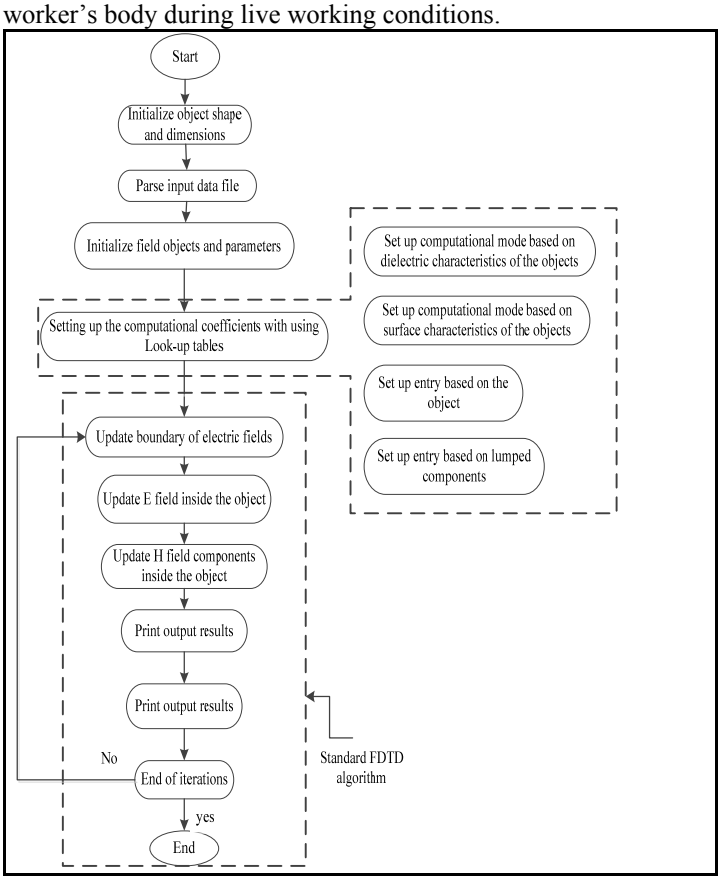

Fig.6: The main steps of the developed FDTD algorithm.

III- Simulation Results

A) *Electromagnetic field distributions over the accessible locations*

With the implementation of the developed algorithm, the magnetic field distribution is calculated. Figure 7 presents the magnetic field distribution over the accessible locations of the worker during live work conditions under 500 kV and 220 kV bus bars at 1 m height level above ground with 50 MW (which presents the average of actual loading conditions) of all outgoing circuits.

The maximum magnetic field is about 10.7 µT (8.52 A/m) under the 500 kV bus bar meanwhile, it reaches about 29.04 µT (23.12 A/m) under the 220 kV bus bar. Based on the charge simulation method the electric field distribution is calculated over the accessible locations of the workers during live work conditions under 500 kV and 220 kV bus bars at 1 m height. The maximum electric field is about 13.5 kV/m under 500 kV bus bar, meanwhile it reaches about 5.93 kV/m under the 220 kV bus bar. The electric field is proportional to the potential value and the higher electric field value reaches under the higher voltage bus bar even if with higher altitude. While the higher magnetic field value reaches under lower voltage bus bar because of proportionality with higher loading currents and lower bus bar altitude.

Figure 8(a, b) presents the electric field distribution under both bus bars of the 500 kV and 220 kV of substation at height level of 1 m above ground. Table 1 presents the maximum magnetic and electric field values and their components with its locations for different working conditions. During bare-hand position in contrast with hot-stick, workers wear special conductive clothing which protects them against the influence of the electric field and this clothing does not protect the live-line worker against the penetration of the magnetic field. The electric field values presented in Table 1 are the maximum values at the location of the workers positions discarding their clothes effects. The maximum magnetic field value imposed to the human body during the bare- hand position is about 7914 µT (6.3 kA/m) while the maximum electric field is about 145 kV/m (without considering the effects of insulating clothes) which are consistent with other related study [13].

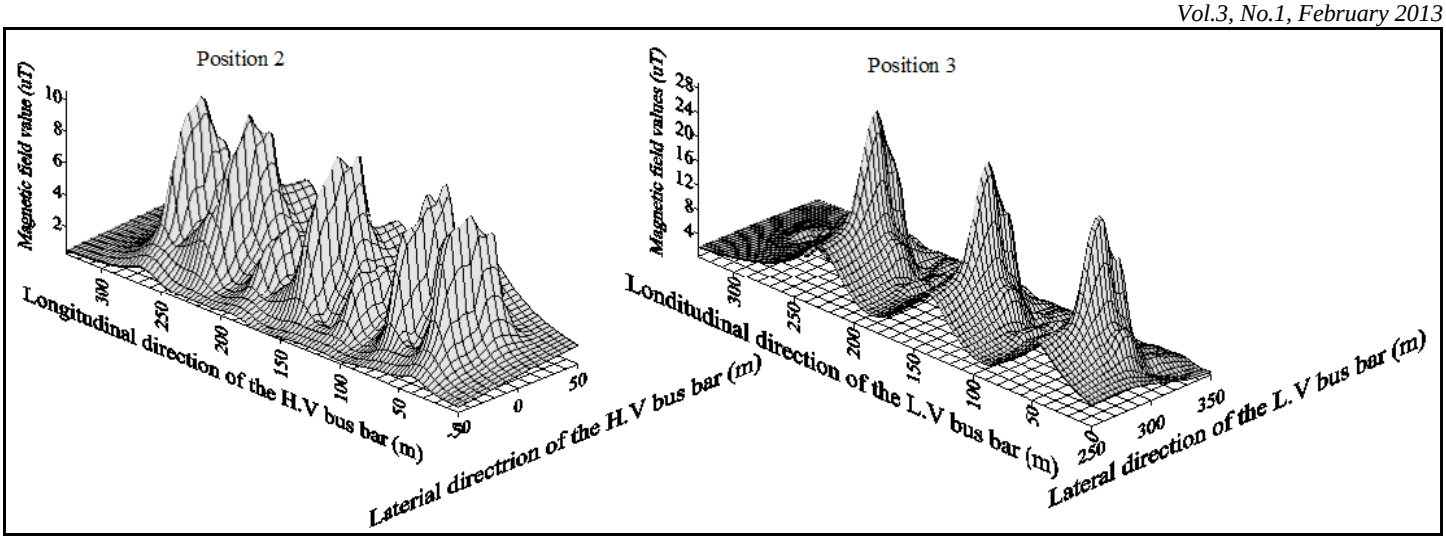

Fig. 7: Magnetic field values (μT) under the bus bars 500 and 220 kV (positions 2&3).

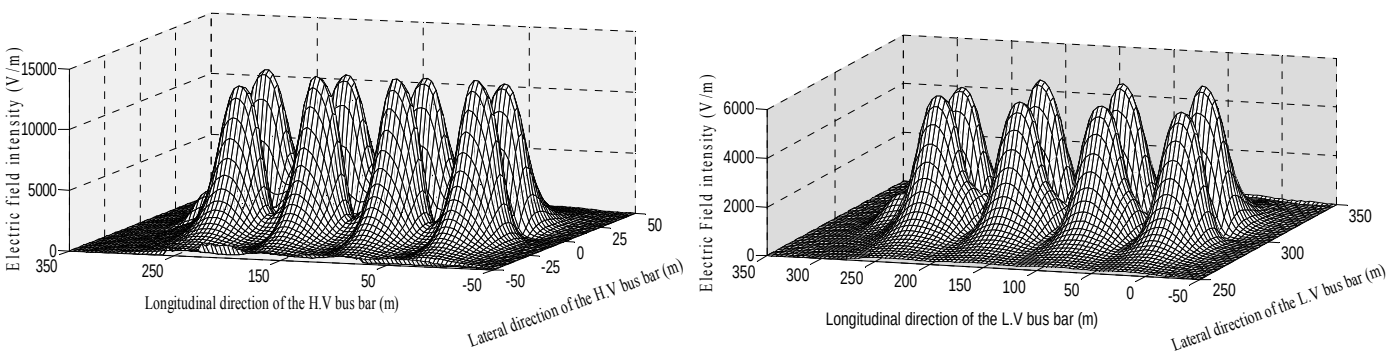

(a) Under 500 kV bus bar (Position 2) (b) Under 220 kV bus bar (Position 3)

Fig.8: Electric field values (V/m) under bus bar 500 and 220 kV (positions 2&3).

Table 1: The maximum magnetic and electric field values at different accessible positions of the workers inside high voltage substation of 500/220 kV

POSITION No.	POSITIONS	Magnetic flux density (uT)				position (m)		Electric field intensity (V/m)				position (m)	
		B_x	B_y	B_z	B_t	Long.	Lat.	E_x	E_y	E_z	E_t	Long.	Lat.
1	*Inside control room (1 m above ground)*	1.18	3.5	9.75	10.43	138	250	15.7	151.3	4146.8	4149.6	126	164
2	*Under 500 kV bus bar (1 m above ground- hot-stick)*	2.3	6.64	8.1	10.7	76	15	42.1	2455.5	13463.8	13685.9	23	-9.5
3	*Under 500 kV bus bar (11 m above ground- bare hand)*	7914	6.67	7.82	7914	231	14	1427.6	109018	95607.8	145009.6	27	-5.3
4	*Under 220 kV bus bar (1 m above ground - hot stick)*	6.83	18.2	21.6	29.04	227	296	18.5	201.7	5924	5927.78	275	290.8
5	*Under 220 kV bus bar (8.5 m above ground- bare hand)*	4710	29.7	31.5	4710.2	135	300	628.4	8957.2	420067	43014.6	281	290.6

B) Absorbed power by worker's skin surface area

The worker's body during live work conditions is exposed simultaneously to both the magnetic and electric field with

power frequency (50/60 Hz). According to power density vector (pointing vector), the absorbed power is given by:

$$P = \mu \left| E \nabla H \right| \quad \text{(Watt/m}^2\text{)} \qquad (11)$$

The worker's different body parts are extracted to calculate the surface area (m^2) of each part. Each part is exposed to the maximum magnetic field values at different accessible position and assumed to be exposed to (1/10) of the maximum electric field values due to the effects of insulating clothes [13]. The electric power absorbed due to simultaneous exposure of electric and magnetic field at different working conditions over the worker's skin surface with (μ_r =0.11) is presented in Table2 in Watts/m^2 for the different human parts. The maximum absorbed power of the worker's body skin surface area is about 11.6 Watt/m^2 under 220 kV bus bar for live line working conditions meanwhile, it reaches to about 6.7 Watt/m^2 under 500 kV bus bar and about 0.82 mWatt/m^2 inside the control room of the substation.

. Table 2: The maximum absorbed power (Watt/m^2) by surface area of human body parts under live work positions

position	Absorbed power by surface area different parts of the worker body at different positions						
	Head (0.08038m^2)	Neck (0.01507m^2)	Chest (0.90432 m^2)	Arm (0.18588 m^2)	Upper leg (0.1758 m^2)	Lower Leg (0.10299 m^2)	Total (Watts)
1	4.5E-5	8.4E-6	0.5E-3	1E-4	9.8E-5	5.8E-5	8.2E--4
2	0.25E-3	4.6E-5	0.003	5.6E-4	5.4E-4	3.1E-4	4.5E-3
3	0.37	0.07	4.2	0.854	0.81	0.473	6.723
4	0.36E-3	6.7E-5	4.0E-3	8.2E-4	7.8E-4	4.6E-4	6.5E-3
5	0.634	0.12	7.2	1.5	1.4	0.82	11.6

C) Total induced current density inside worker's body.

The total induced electric current density inside the different worker's body parts is calculated due to the exposure of both electric and magnetic field simultaneously. The electric potentials are calculated at the surface of the worker's body and consequently the induced electric is calculated as the type of the simulation charges to calculate the field components while the magnetic field induces secondary electric field as secondary field components. Vector summation of the components for the primary and secondary fields is performed inside each worker's body parts and consequently the total induced field is obtained. The main different physical properties of the worker's body parts are tabulated in Table 3. The total induced current density is calculated as ($J = \sigma E$ A/m^2) during the different live work accessible positions. Table 4 presents the total induced current density (A/m^2) inside the different worker's body at the two accessible positions (Hot-sticks and Bare hand) under the 500 kV and 220 kV bus bars. The maximum induced current density reaches about 2.45 mA/m^2 inside the worker's head under 500 kV for bare hand position while it reaches about 2.27 mA/m^2 under 220 kV bus bar for bare hand position. These values are due to higher induced electric fields and higher brain conductivity (0.7 ($\Omega^{-1}m^{-1}$).

Table 3: Tissue conductivity and permittivity values [22]

Tissue	Conductivity σ ($\Omega^{-1}m^{-1}$)	Relative Dielectric constant ε_r
Muscle	0.86	434930
Bone	0.04	12320
Skin	0.11	1136
Heart	0.5	352850
Gland	0.11	56558
Blood	0.6	5259
Lung	0.04	145100
Liver	0.13	85673
Lens	0.11	105550

Table 4: The total induced current density inside the worker's parts for different positions under 500 kV and 220 kV bus bars.

Parts	Under 500 kV Bus bar				Under 220 kV Bus bar			
	hot-stick position		bare-hand position		hot-stick position		bare-hand position	
	E(μV/m)	J (μA/m2)	E(μV/m)	J (μA/m2)	E(μV/m)	J (μA/m2)	E(μV/m)	J (μA/m2)
Head	191.4	53.2	8829.4	2453.7	225.8	62.7	8194.7	2277.4
Neck	134.1	37.3	618.1	171.7	158.1	4.4	5736.3	159.4
Chest	382.9	36.1	15650	1472.7	451.6	42.5	16824	1583.2
Arm	95.1	9.5	414.6	414.6	112.2	11.2	4698	469.8
Upper leg	153.1	15.3	3436.2	343.6	180.7	18.1	3438.2	343.8
Lower leg	95.7	9.6	2147.6	214.7	112.9	11.3	2148.8	214.8

D) Electromagnetic fields variation over human organs.

The FDTD computational region is divided into cells as Yee cell with the corresponding electric and magnetic fields being located on the edges and the faces. It assumed that all field values in the entire solution region are the maximum computed electric and magnetic fields at the accessible locations of the worker's during live working conditions. Worker's vital organ (brain) is defined by specifying the dielectric parameters at each discrete location in the FDTD mesh. The computational region must be large enough to enclose the objects to be analyzed. In addition, suitable boundary conditions on the artificial boundary must be imposed to absorb outgoing waves to simulate the extension of

the computational region to infinity. The discretization and time steps are accordingly adjusted based on the organ dimensions and type of source, its frequency and wavelength. To ensure the stability of the algorithm, the discretization step is assumed to be $\Delta x=10^{-12}$ m while the time step is assumed as:

$$\Delta t = \left(\frac{\Delta x}{2.c}\right) \quad \text{Sec.} \tag{12}$$

Where c: is the light speed = $3*10^8$ m/s

These conditions with very low frequency (f= 60/50) Hz yield to very long wavelength (λ=c/f in meters) of the simulated harmonic electric and magnetic dipole sources as:

$$F(t) = F_{\max}.\cos\left(\frac{2\pi.c}{\lambda}t\right) \tag{13}$$

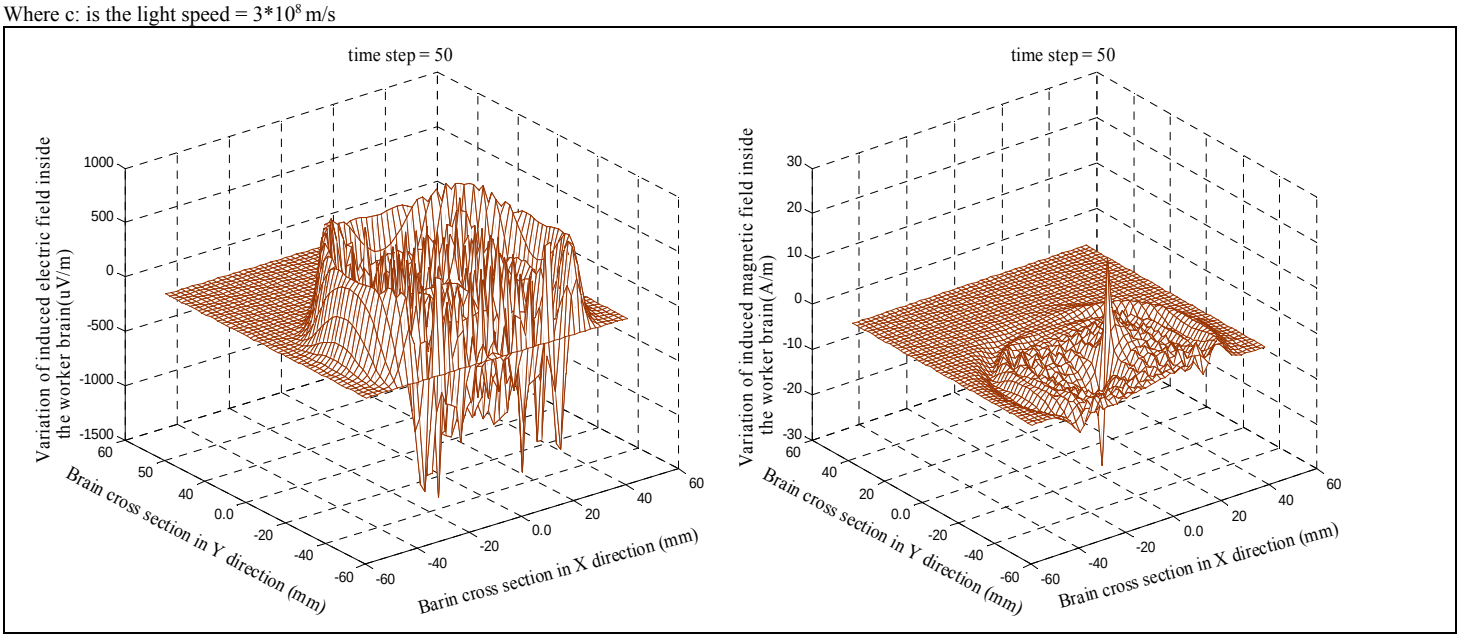

Fig.9: Variation of electric and magnetic fields penetrating the worker brain's cross section during the bare-hand positions at time step=50.

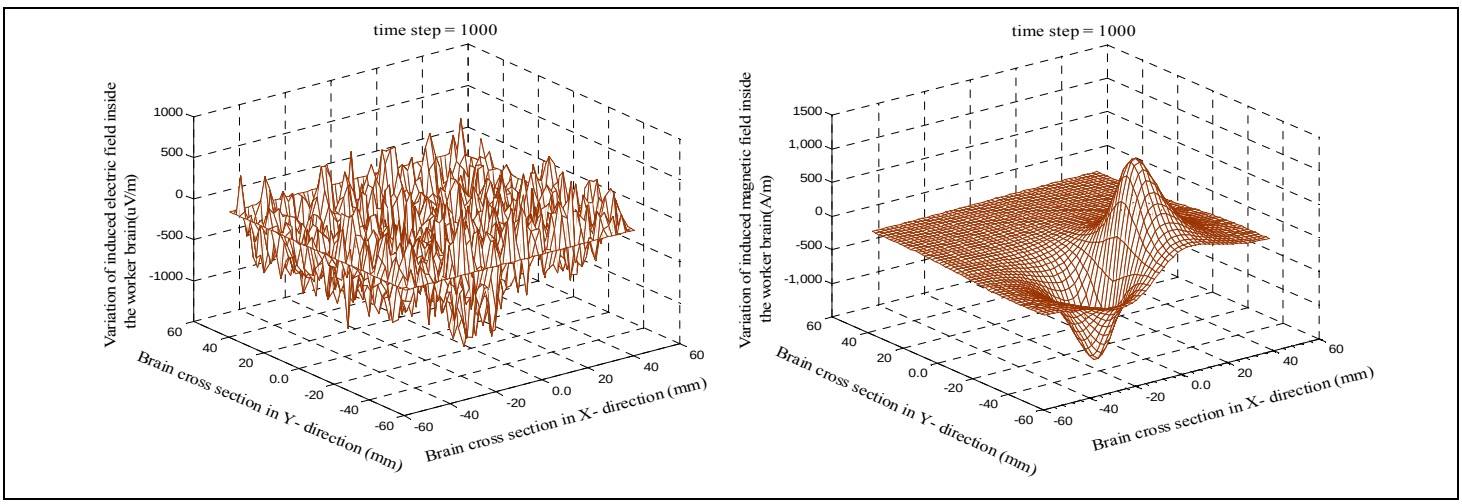

Fig.10: Variation of electric and magnetic fields penetrating the worker brain's cross section during the bare-hand positions at time step=1000.

A very small time incrimination is adjusted to enable the algorithm to capture and monitor the variation of electric and magnetic fields penetrating worker's organ such as the worker's brain.

$$\lambda = N_{\lambda} * \Delta x \tag{14}$$

Where N_{λ}: is the No. of points per wavelength.

The worker brain is simulation as a sphere of 6 cm radius and is positioned in a grid of cubic block to establish FDTD meshing grid of very small step ($\Delta x=\Delta y=\Delta z= 10^{-12}$ m). Figure 9 and Figure 10 present the variations of electric and magnetic fields that penetrate the worker's brain during live work under 500 kV bus bar (bare hand position) at different time steps. The electric field is imposed to higher attenuation factor than magnetic field because of the physical properties of the brain and the magnetic field almost see the human organ as transparent rather than the electric field.

IV- CONCLUSIONS

Typical high voltage substation 500/220 kV is simulated to calculate individually the magnetic and electric fields. Moreover, analytical worker's body model is developed and is allocated in different accessible locations during live work inside the substation. The maximum magnetic field value imposed to the human body during the bare- hand position is about 7914 µT (6.3 kA/m) while the maximum electric field is about 145 kV/m (without considering the effects of insulating clothes). The maximum induced current density reaches about 2.45 mA/m^2 inside the worker's head under 500 kV for bare hand position while it reaches about 2.27 mA/m^2 under 220 kV bus bar for bare hand positions. The maximum absorbed power of the worker's body skin surface area is about 11.6 Watt/m^2 under 220 kV bus bar and it reaches to about 6.7 Watt/m^2 under 500 kV bus bar. The electric and magnetic fields penetrating the worker's organs are captured over the worker brain using the FDTD algorithm with very small frequency (50/60 Hz) and very long harmonic dipole source wavelengths.

V- REFERENCES

[1] Khaled Ellithy, Abdulaziz Al Shafai and Fahad Al Assiry," Measurement of Magnetic Fields in an Outdoor High Voltage Power Substation" , North American Power Symposium (NAPS), 2009 .

[2] A. S. Safigianni and C. G. Tsompanidou, "Electric and Magnetic Field Measurements in an Outdoor Electric Power Substation", IEEE Trans. Power Delivery. Vol. 24, No. 1, pp. 38-42, January 2009.

[3] WHO - World Health Organization. Extremely low frequency fields. Environmental Health Criteria, Vol. 238. Geneva, World Health Organization, 2007.

[4] "EMF Design Guidelines for Electric facilities", Report, Southern California Edison Company (SCE), Sept 2004.

[5] "IEEE Standard Procedures for Standard Procedures for measurements of Electric and Magnetic Fields from AC Power Lines", New York, IEEE, ANSI/IEEE Std. 644.

[6] 'Directive 2004/40/EC of the European Parliament and of the Council of 29th April 2004 on the minimum health and safety requirements regarding the exposure of workers to the risk arising from physical agents (electromagnetic fields) (18th individual Directive within the meaning of Article 16(1) of Directive 89/391/EEC)', Official Journal of the European Union, 2004, Nr. L 184, pp. 1–9.

[7] International Commission on Non-Ionizing Radiation Protection: 'Guidelines for limiting exposure to time-varying electric, magnetic, and electromagnetic fields (up to 300 GHz)', Health Phys., 1998, 74, (4), pp. 494–521.

[8] C. Munteanu, G. Visan, I. T. Pop, V. Topa, E. Merdan, A. Racasan, "Electric and Magnetic Field Distribution inside High and Very High Voltage Substations" (Proc. 20th International Zurich Symposium on Electromagnetic Compatibility, pp. 277-280, Ian. 2009).

[9] Calin Munteanu., et al.," Electric and Magnetic Field Distribution Inside High Voltage Power Substations. Numerical Modeling and Experimental Measurements", ieej transactions on electrical and electronic engineering ieej trans 2010.

[10] A. S. Safigianni and C. Tsompanidou, " Measurements of the Electric and Magnetic Fields Due to the Operation of Indoor Power Distribution Substations ", 38th International Universities Power Engineering Conference UPEC 2003, Thessaloniki, Greece, September 2003.

[11] Fahs, H., Lanteri, S., Wiart, J. and Man-Fai Wong," Calculation of the SAR induced in head tissues using a high order DGTD method and triangulated geometrical models," Electromagnetic Theory (EMTS), 2010 URSI International Symposium on Fields, Waves & Electromagnetics, 2010 , pp 547 – 550.

[12] S. Fiori, A. Faba, L. Albini, E. Cardelli, and P. Burrascano," Numerical modeling for the localization and the assessment of electromagnetic field sources", Magnetics IEEE Transactions, Volume: 39 , Issue: 3 , Part: 1, 2003 , pp 1638 – 1641.

[13] W. Krajewski ," Numerical assessment of electromagnetic exposure during live-line works on high-voltage objects ", Science Measurement & Technology IET , Volume: 3 , Issue 1 , 2009 , Page(s): 27 – 38.

[14] Egyptian Electrical Authority Live Working Committee Text Book for Working Conditions of 66, 132, 220, 500 kV lines. Talkha Center of Live-Line Maintenance.

[15] H. Anis, M.A. Abd-Allah and Sh. A. Mahmoud, "Computation of Power Line Magnetic Fields - A Three Dimensional Approach", 9th International Symposium on High Voltage Engineering (ISH1995), paper 8333, Aug/Sept.1995.

[16] Nazar H. Malik, "A review of the charge simulation method and its applications" IEEE Transactions on Electrical Insulation, vol. 24, no. 1, pp. 3–20, February 1989.

[17] Masanori Akazaki and Kiyoto Mishijima, "Calculation of three dimensional axisymmetric fields by charge simulation method", Electrical Engineering in Japan, vol. 98 no. 4, pp.1–7, July 1978.

[18] J. H. Pickles, "Monte-Carlo Calculation of Electrically Induced Human-Body Currents" IEE Science Proceedings, Vol. 134, Pt. A, No. 9, pp. 705-711, November 1987.

[19]. A. Taflove, Computational Electrodynamics, The Finite Difference Time Domain Approach, Third Ed., Artech House, Norwood, MA, 2005.

[20]. A. Bondeson, T. Rylander, and P. Ingelström, Computational Electromagnetics, Springer, New York, 2005, Series: Texts in Applied Mathematics , Vol. 51., pp. 58-86.

[21] G. Mur, "Absorbing boundary conditions for the finite-difference approximation of the time-domain electromagnetic field equations," IEEE Trans. Electromagn. Compat., vol. EMC-23, no. 4, pp. 377-382, Nov. 1981.

[22] M. Bencsik, R. Bowtell and R. Bowley, "Electric Fields Induced in the Human Body by Time-Varying Magnetic Field Gradients in MRI: Numerical Calculations and Correlation Analysis" Journal of Appl. Phys.: Phys. Med. Biol. Vol. 52, pp. 2337-2353, 2007